

BP Neural Network and improved Particle Swarm Optimization for Transient Electromagnetic Inversion

Huaiqing Zhang*, Ruiyou Li, Nian Yu, Ruiheng Li, Qiong Zhuang

The State Key Laboratory of Transmission Equipment and System Safety and Electrical New Technology, Chongqing University, Chongqing, 400044, China

zhanghuaiqing@cqu.edu.cn (Huaiqing Zhang); 1378546842@qq.com (Ruiyou Li); 61408155@qq.com (Nian Yu); 392361773@qq.com (Ruiheng Li); 779695034@qq.com (Qiong Zhuang)

*Correspondence to: zhanghuaiqing@cqu.edu.cn

Abstract. As one of the most active nonlinear inversion methods in transient electromagnetic (TEM) inversion, the back propagation (BP) neural network has high efficiency because the complicated forward model calculation is unnecessary in iteration. The global optimization ability of the particle swarm optimization (PSO) is adopted for amending BP's sensitivity on initial parameters, which avoids it falling into local optimum. A chaotic oscillation inertia weight PSO (COPSO) is proposed in accelerating convergence. The COPSO-BP algorithm performance is validated by two typical testing functions, ~~and~~ then by two geoelectric models inversion and a field example. The results show that the COPSO-BP method has better accuracy, stability and relative less training times. The proposed algorithm has a higher fitting degree for the data inversion, and it is feasible in geophysical inverse applications.

Keywords: transient electromagnetic inversion; BP neural network; particle swarm optimization; chaotic oscillation

1 Introduction

Transient electromagnetic (TEM) method applies the secondary receiving voltage induced by the rapid switching off pulse current, and then deduces the geoelectric structure parameters. The later is a typical TEM inversion issues with nonlinear feature. The linear inversion method was simple and widely used through linearization process, yet it is extremely dependent on initial parameters selection and resulting in poor inversion accuracy. Hence, the nonlinear inversion methods attract more geophysicists attention in recent years.

The artificial neural network(ANN) is one of the most active nonlinear inversion methods, it has very high computation efficiency because the complicated forward model calculation is unnecessary in iteration. All the geoelectric parameters and the forward model relations are

Conflicts of Interests

The authors declare that they have no conflict of interest.

31 implied in the weight and threshold parameters of ANN. And it is different from the non-linear
32 Monte Carlo method with global space search solution (He et al., 2018; Jha et al., 2008; Pekşen et
33 al., 2014; Sharma, 2012; Tran and Hiltunen, 2012). Srinivas et al. (2012) compared the inversion
34 performance of BP, radial basis function(RBF) and generalized regression neural network (GRNN)
35 in vertical electrical sounding data, then established a 1-D inversion model with BP and finally
36 realized the parameters inversion. Maiti et al. (2012) proposed a Bayesian neural network training
37 method in 1-D electrical sounding. Jiang et al. (2018) improved the training method for kernel
38 principal component wavelet neural network and achieved the resistivity imaging. Jiang et al.
39 (2016a) gave a learning algorithm based on information criterion (IC) and particle swarm
40 optimization for RBF network which improves the global search ability. Johnson (2017) utilized
41 neural network method to invert multi-layer georesistivity sounding. Jiang et al. (2016b) presented
42 a pruning Bayesian neural network (PBNN) method for resistivity imaging and solved the
43 instability, local minimization problems. Raj et al. (2014) solved non-linear apparent resistivity
44 inversion problems with ANN. The ANN has been widely applied in electric prospecting data
45 interpretation for its powerful fitting ability. However, the neural network method is sensitive to
46 initial parameter settings and falls easily into local minimum. Lots improved methods were
47 proposed for balancing the convergence rate and inversion quality. Zhang and Liu (2011) proposed
48 ant colony optimization for ANN and applied in high density resistivity, acquired smaller
49 inversion errors and higher determinant coefficients. Dai et al. (2014) suggested a differential
50 evolution (DE) for BP which enhanced the global search ability. Marina et al. (2014) introduced
51 the genetic algorithm for ANN.

52 The Particle swarm optimization (PSO) has simple structure, fast convergence rate, high
53 accuracy and global optimization ability. [FernándezFernandez](#) et al. (2010) successfully introduced
54 the PSO in 1-D resistivity inversion. Godio and Santilano (2018) applied it in geophysical
55 inversion and deduced a depth resistivity earth model. Since the PSO's global searching
56 performance, the BP's initial weights and thresholds can be trained by PSO and then the BP's
57 global optimization ability can be improved. Comparing to the standard PSO (SPSO), a chaotic
58 oscillation inertia weight PSO (COPSO) which can accelerate the convergence rate in the early
59 stage was proposed naturally([Shi et al., 2009](#)).

60 The paper structure is as following: the principle of PSO algorithm with different inertia
61 weights schemes, the BP neural network and the proposed COPSO-BP algorithm are given in
62 section 2. Then, the COPSO-BP algorithm performance is validated by two typical testing
63 functions in section 3. And in later section, inversion simulations of a three-layer and five-layer
64 geoelectric models are carried out, the hidden layer neuron numbers determining method is put
65 forward and algorithms performance is compared.

66 **2 Principle of COPSO-BP Algorithms**

67 **2.1 Chaotic Oscillation PSO algorithm**

68 For N -dimensional optimization problem, supposing the position (resistivity and thickness for
69 layered model parameters inversion) and velocity(update speed) of the i -th particle (global search
70 group number) at time t are $x_i = (x_{i1}, x_{i2}, \dots, x_{iN})$ and $v_i = (v_{i1}, v_{i2}, \dots, v_{iN})$ respectively. Then, at time
71 $t+1$, they can be calculated by the iterations as

72
$$v_{id}^{t+1} = \omega \cdot v_{id}^t + c_1 r_1 (p_{id}^t - x_{id}^t) + c_2 r_2 (p_{gd}^t - x_{id}^t) \quad (1)$$

73
$$x_{id}^{t+1} = x_{id}^t + v_{id}^{t+1} \quad (2)$$

74 where r_1, r_2 are random value evenly distributed in the interval $(0,1)$, c_1, c_2 are learning factors
75 (usually equal to 2). And p_{id}, p_{gd} means the individual and global maximum.

76 The inertia weight parameter ω affects the algorithm performance seriously. A fixed weight
77 always was used in the early time, and then various dynamic weights were proposed. Shi et al.
78 (2010) have summarized several methods as

79
$$\omega_1(t) = \omega_s - (\omega_s - \omega_e) t / T_{\max} \quad (3)$$

80
$$\omega_2(t) = \omega_s - (\omega_s - \omega_e) (t / T_{\max})^2 \quad (4)$$

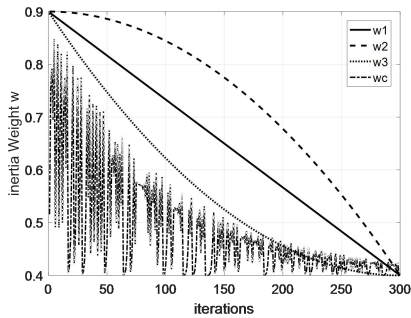
81
$$\omega_3(t) = \omega_s - (\omega_s - \omega_e) [2t / T_{\max} - (t / T_{\max})^2] \quad (5)$$

82 Where ω_s and ω_e are the start and end weight. The t, T_{\max} are the current and maximum iteration.
83 The above weights are of smooth and monotonically decreasing. In this paper, we proposed a
84 decreasing oscillation weights scheme which was based on chaotic logistic equation. Its specific
85 calculation formula as

86
$$x_{t+1} = \mu x_t (1 - x_t) \quad t = 0, 1, 2, \dots, n \quad (6)$$

87
$$\omega_c(t) = \omega_e + (\omega_s - \omega_e) (0.99^t \cdot x_t) \quad (7)$$

88 where μ is the control parameter. A complete chaos state is established for $x \in (0,1)$ and $\mu = 4$, an
89 inertia weight is then obtained from Eq.(7). Numerical experiments were carried out
90 correspondingly and showed that the initial value of x_0 has little effect on inertia weight ω . The
91 inertia weights comparison was shown in Fig.1 where $x_0 = 0.234$ and $\mu = 4$ for chaotic oscillation.



92

93

Fig. 1 Inertial weight curves comparison

94

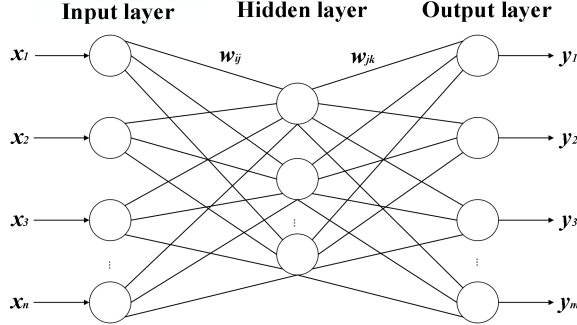
2.2 BP Neural Network

95

BP neural network is multi-layer feed forward structure, and a typical three-layer network is

96

shown in Fig. 2 (Yong et al., 2009).



97

98

Fig. 2 Three-layer BP neural network structure

99

where x_1, x_2, \dots, x_n are the input value, y_1, y_2, \dots, y_m are the predicted output, w_{ij}, w_{jk} are the network

100

weights. The threshold parameter α is defined in hidden layer with its output

101

$$H_j = f\left(\sum_{i=1}^n w_{ij}x_i - \alpha_j\right) \quad j = 1, 2, \dots, l \quad (8)$$

102

where l is the hidden layer nodes numbers, f is the activation function with different expressions,

103

and the most widely used is sigmoid type function. The predicted output for the k -th unit is

104

calculated by

105

$$O_k = \sum_{j=1}^l H_j w_{jk} - b_k \quad (9)$$

106

And parameter b means the output threshold. Then the prediction error can be determined based

107

on predicted output O_k and the expected output T_k as $e_k = (T_k - O_k)O_k(1 - O_k)$. The updating formula

108

for weights and thresholds are as following

109

$$\begin{cases} w_{ij} = w_{ij} + \eta H_j (1 - H_j) x_i \sum_{k=1}^m w_{jk} e_k \\ w_{jk} = w_{jk} + \eta H_j e_k \\ \alpha_j = \alpha_j + \eta H_j (1 - H_j) \sum_{k=1}^m w_{jk} e_k \\ b_k = b_k + e_k \end{cases} \quad (10)$$

110

where $i=1, 2, \dots, n; j=1, 2, \dots, l; k=1, 2, \dots, m$; and η is the learning rate.

111

2.3 BP Neural Network with COPSO algorithm

112

The initial parameters are chosen randomly, which affects the convergence rate, learning

113

efficiency and perhaps falling into local minimum. The Chaotic Oscillation PSO (COPSO) has a

114

much better global optimization capability, therefore, we proposed the COPSO algorithm for BP

115

parameters' training. The COPSO-BP pseudo-codes were briefly described as following:

116

117 **Table.1** Pseudo-codes of COPSO-BP algorithm

```

1:  BP network structure definition (neuron numbers  $n,l,m$ , and activation function)
2:  COPSO initialization for BP (weights, threshold as  $X$ . PSO parameters as  $V_{\min}, V_{\max}, \omega_c, c_1, c_2$ , size  $M$ ,  $T_{\max}$ )
3:  Initializing BP with  $X_i$  ( $i=1,2,\dots,M$ ) and evaluating fitness by Eq.(11) for each individual
4:  Setting the  $p_{id}$  and  $p_{gd}$ 
5:  While  $iter < T_{\max}$  do
6:      updating inertia weight by Eq.(7)
7:      for  $i=1:M$  (all particles) do
8:          updating velocity  $V_i$  by Eq.(1)
9:          updating particle position  $X_i$  by Eq.(2)
10:         Initializing BP with new  $X_i$  and calculating fitness by Eq.(11)
11:         if  $X_i$  is better than  $p_{id}$ 
12:             Set  $X_i$  is to be  $p_{id}$ 
13:         End if
14:         if  $X_i$  is better than  $p_{gd}$ 
15:             Set  $X_i$  is to be  $p_{gd}$ 
16:         End if
17:     End for  $i$ 
18:      $iter = iter+1$ 
19: End While
20: Initializing BP with  $p_{gd}$ 
21: Inputting and obtaining the predicted output

```

118 The formula for calculating the i -th particle fitness is defined as

$$119 \quad f_i = \frac{1}{S} \sum_{s=1}^S \sum_{j=1}^m (Y_{sj} - \hat{Y}_{sj})^2 \quad (11)$$

120 where S is the number of training set samples, m is the output neurons number, Y_{sj} is the j -th
121 ~~reference~~ true output of the s -th sample, and \hat{Y}_{sj} is the corresponding predict output.

122 3 Algorithm Testing

123 In order to investigate the COPSO-BP performance and reliability, two typical testing functions
124 were adopted and simulations were performed in MATLAB.

125 (1) *Rosenbrock* function:

$$126 \quad f_1 = 100 \times (x_1^2 - x_2)^2 + (1 - x_1)^2, x_i \in [-10, 10], i = 1, 2 \quad (12)$$

127 (2) *Bohachevsky* function:

128 $f_2(x) = x_1^2 + x_2^3 - x_1x_2x_3 + x_3 - \sin(x_2^2) - \cos(x_1x_3^2), x_i \in [-2\pi, 2\pi], i = 1, 2, 3$ (13)

129 The standard PSO-BP (SPSO-BP) with linear decreasing inertia weight as Eq.(3), the
 130 COPSO-BP were carried out respectively. The three-layer BP of $n-s-1$ structure is constructed with
 131 different hidden nodes. The PSO parameters are population size $M = 60$, learning factors $c_1 = c_2 =$
 132 2.0 , the maximum iteration $T_{\max} = 30$, inertia weight $\omega_s = 0.9$, $\omega_e = 0.4$, $x_0 = 0.234$ and $\mu = 4$ for
 133 chaotic parameters, the search dimension $D = n \times s + s \times 1 + s + 1$ which includes all the neuron
 134 weights and thresholds. For BP network, 150 training samples and 50 testing samples were
 135 randomly produced within the variable range. The training error is defined as

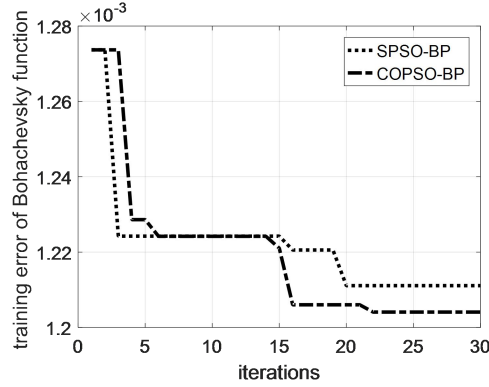
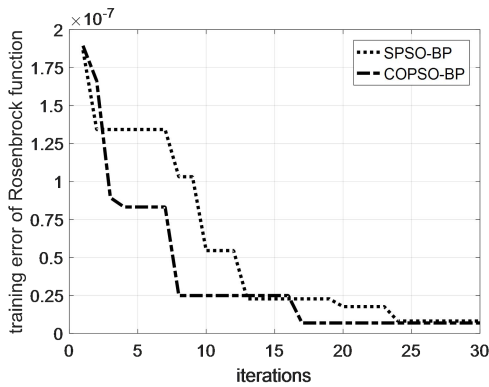
136 $E = \frac{1}{S} \sum_s (T_s - O_s)^2$ (14)

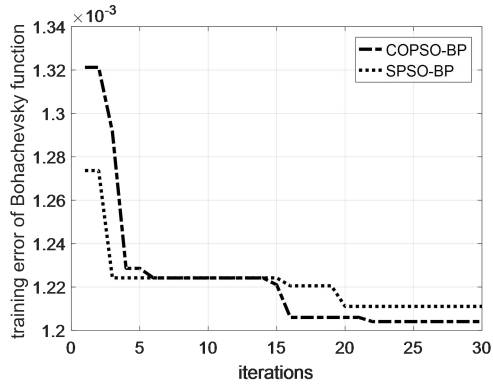
137 where S is the training samples number, T_s, O_s are the expected and predicted output for training
 138 sample s respectively. The network structures with minimum training errors for *Rosenbrock* and
 139 *Bohachevsky* functions are 2-7-1 and 3-6-1 respectively. The simulation performs 20 times for
 140 each testing function with SPSO-BP and COPSO-BP algorithms. The numerical result was shown
 141 in Table.2. One of the evolutionary training error curves were shown in Fig.3, and the fitting
 142 curves of COPSO-BP algorithm were shown in Fig.4.

143 **Table.2** Comparison of SPSO-BP and COPSO-BP algorithm for testing functions

Testing functions	SPSO-BP		COPSO-BP	
	Average value	Optimal value	Average value	Optimal value
<i>Rosenbrock</i>	2.375e-3	2.300e-5	5.226e-3	2.410e-06
<i>Bohachevsky</i>	0.225	1.024e-3	0.193	3.360e-4

144

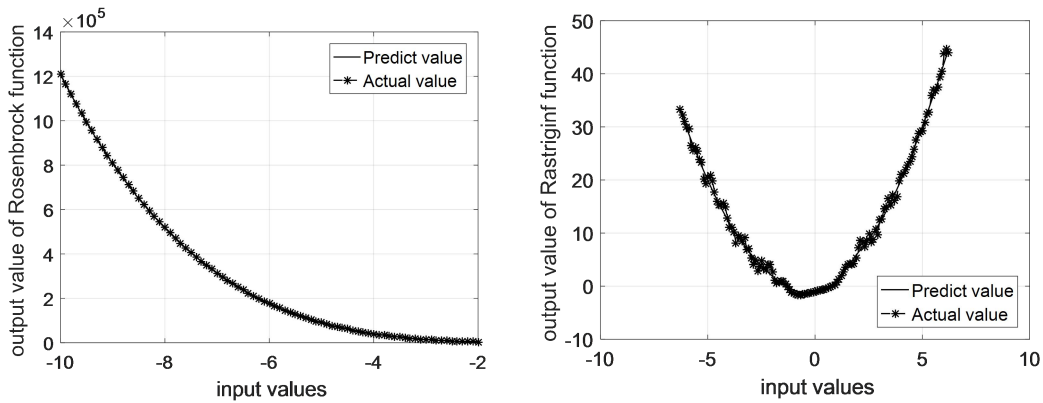




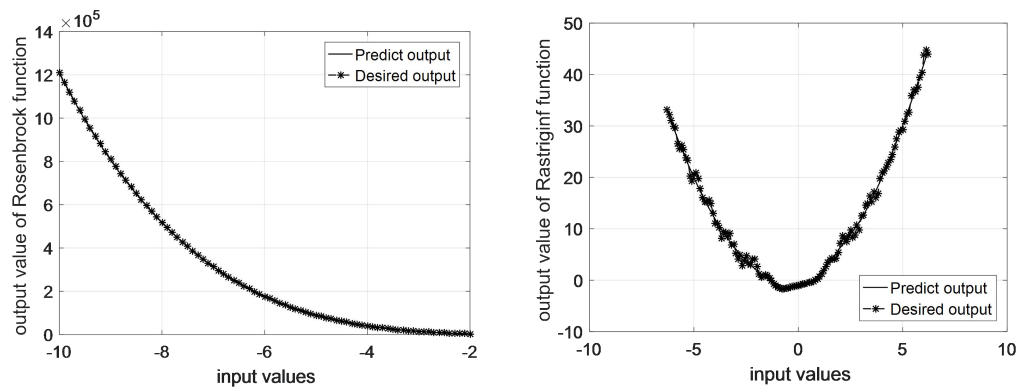
145

146

Fig. 3 Training error curves of SPSO-BP and COPSO-BP algorithms



147



148

149

Fig. 4 Fitting curves of COPSO-BP algorithm

150

151

152

153

154

It can be seen in Table.2 that both the SPSO-BP and COPSO-BP algorithms can acquire a relative high accuracy for testing functions, the COPSO-BP is a ~~slightly better~~ better than SPSO-BP. However, the COPSO-BP has better convergence rate and optimization efficiency in the early stage in Fig.3. Therefore, the SPSO-BP and COPSO-BP algorithms have strong learning ability, good stability and generalization ability, which will be suitable for TEM inversion.

155

4 Layered model and parameter analysis

156

4.1 Forward Model

157

158

According to Kaufman's derivation (1983), the frequency response of central loop source for the layered model takes the following Hankel transform

$$159 \quad H_z(\rho, \omega) = Ia \int_0^{\infty} \frac{m^2}{m + m_1/R_1^*} J_1(m\rho) dm \quad (15)$$

160 where a is the radius of transmitting coil, I is the excitation current, ρ is the center distance
 161 between the transmitting coil and the receiving coil, $J_1(m\rho)$ is the first-order Bessel function, m
 162 is integral variable, $m_1 = (m^2 - k_1^2)^{1/2}$, k_1 is the conduction current, σ_1 is the conductivity, $k_1 = -i\omega\mu\sigma_1$,
 163 and R_1^* is the first layer apparent resistivity conversion function which can be obtained by the
 164 following recurrence formula

$$165 \quad \begin{cases} R_n^* = 1 \\ R_j^* = \frac{m_j R_{j+1}^* + m_{j+1} \text{th}(m_j h_j)}{m_{j+1} + m_j R_{j+1}^* \text{th}(m_j h_j)} \end{cases} \quad (16)$$

166 There is no analytical solution for the time-domain response for layered model, it can only be
 167 solved by numerical calculation. The Hankel transform in formula (15) ~~can be~~ calculated by ~~fast~~
 168 ~~algorithm as an improved digital filtering algorithm with 47 points J_1 filter coefficient~~ ~~filter method~~,
 169 and then time response can be obtained using the Gaver-Stehfest transform as follows:

$$170 \quad H_z(\rho, t) = \frac{\ln 2}{t} \sum_{n=1}^N K_n H_z(\rho, s_n) \quad (17)$$

171 where $s_n = (\ln 2/t) \times n$, K_n is the coefficient, N is determined by the computer bits, generally $N=12$.

172 The ramp excitation current of TEM is

$$173 \quad I(t) = \begin{cases} 0, & t < 0 \\ t/T_1, & 0 \leq t < T_1 \\ 1, & T_1 < t \end{cases} \quad (18)$$

174 where T_1 is the turn-off time, and the Laplace transform is

$$175 \quad I(s) = \frac{1}{T_1 s^2} - \frac{1}{T_1 s^2} e^{-T_1 s} = \frac{1}{T_1 s^2} (1 - e^{-T_1 s}) \quad (19)$$

176 Therefore, for a specific layered model, the apparent resistivity conversion function R_1^* is firstly
 177 calculated by recurrence formula (16) based on geoelectric structure parameters. And then the
 178 frequency response at fixed point $H_z(\omega)$ is calculated by Hankel transform as formula (15). For
 179 ramp excitation, the Laplace transform of $H_z(s)$ should multiplied by $I(s)$. Finally, the time
 180 response $H_z(t)$ is obtained by Gaver-Stehfest transform as formula (17). So the $H_z(t)$ is obtained by
 181 a Gaver-Stehfest transform, a Hankel transform and a recurrence calculation, and it is somewhat
 182 heavy computational consuming.

183 However, the vertical magnetic field $H_z(t)$ is the actual observed signal in transient
 184 electromagnetic method in engineering applications. It is the inversion input and output is
 185 geoelectric structure parameters. A method which can avoid the complicated forward model
 186 calculation is of great importance in algorithm efficiency.

187 4.2 BP network design and COPSO algorithm

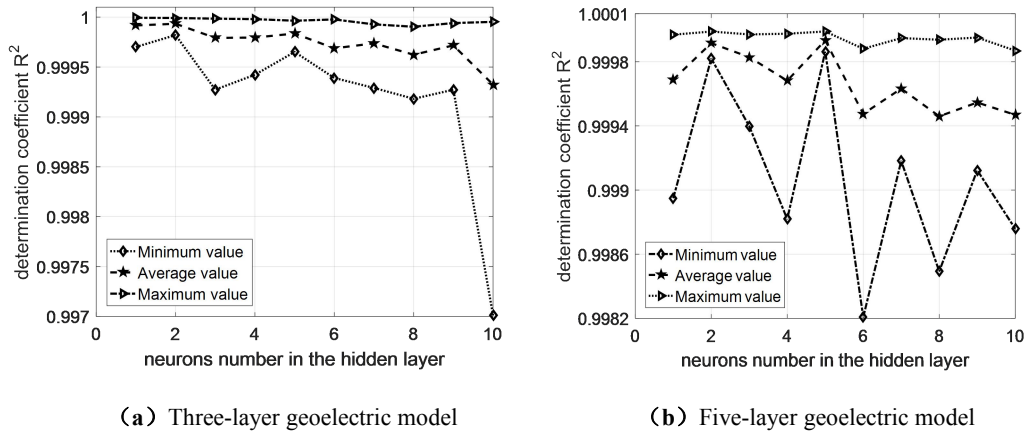
188
189
190
191
192
193
194
195
196
197
198

For BP structure, the output nodes are determined by the number of inversion geoelectric parameters, the input nodes are determined by the samples number of $H_z(t)$, the hidden nodes varies according to approximation performance. As a three-layer or five-layer geoelectric model, its geoelectric parameters are 5 (three resistivity and two thickness parameters) or 9 (five resistivity and four thickness parameters), the output nodes are 5 or 9 correspondingly. The characteristic samplings of $H_z(t)$ are chosen as 10 or 20, which are determined by the model's complexity, more layers mean mores sampling points needed. The 10 samplings were selected in this paper hence with 10 input nodes. While for the hidden layer neuron, its number is related to the weights and threshold parameters amount directly and affects the BP performance greatly. An appropriate hidden nodes number is necessary and a determination coefficient R^2 is defined for evaluating as

$$R^2 = \frac{\left(n \sum_{i=1}^n Y_i \hat{Y}_i - \sum_{i=1}^n Y_i \sum_{i=1}^n \hat{Y}_i \right)^2}{\left(n \sum_{i=1}^n \hat{Y}_i^2 - \left(\sum_{i=1}^n \hat{Y}_i \right)^2 \right) \left(n \sum_{i=1}^n Y_i^2 - \left(\sum_{i=1}^n Y_i \right)^2 \right)} \quad (20)$$

200
201
202
203
204
205
206

where Y_i is the ~~reference value~~ true value, \hat{Y}_i is the predicted value for i -th training data, n is the training data number. A larger determination coefficient means a better approximation performance. The simulations on hidden nodes effect were carried out for a three-layer and five-layer geoelectric models. The BP structure is 10- s -5 and 10- s -9, its transfer, training and learning functions are 'Log sigmoidal', 'Levenberg-Marquardt' and 'Gradient descent momentum' respectively. The average, minimum and maximum value of R^2 were obtained after running 20 times for each simulation. The R^2 curves were shown in Fig.5.



207
208
209
210
211
212
213

Fig. 5 Influence of hidden layer nodes on R^2 for different geoelectric model

It can be seen that the optimal neural network structures were 10-2-5 and 10-5-9 for three and five-layer models based on the maximum R^2 . Then, the PSO-BP algorithms with different inertia weight were implemented and compared for three-layer model. The BP structure was chosen as 10-2-5, four types of inertia weight as Eq. (3~7) in PSO were compared in Table.3.

214 **Table.3** Comparison of different inertia weights in PSO algorithms ($\omega_s = 0.9, \omega_c = 0.4$)

inertia weight	iteration number	minimum fitness	average fitness	convergence time(s)
ω_1	9	1.3914e-3	1.3982e-3	65.21
ω_2	29	1.4406e-3	1.4418e-3	204.97
ω_3	25	1.4168e-3	1.4224e-3	189.17
ω_c	6	1.3846e-3	1.3925e-3	44.34

215 The simulation was implemented on Core (TM) i5-7500 with 8GB memory. It is obviously
 216 found in Table.3 that the COPSO algorithm has much faster convergence rate, less iteration
 217 number and time consuming.

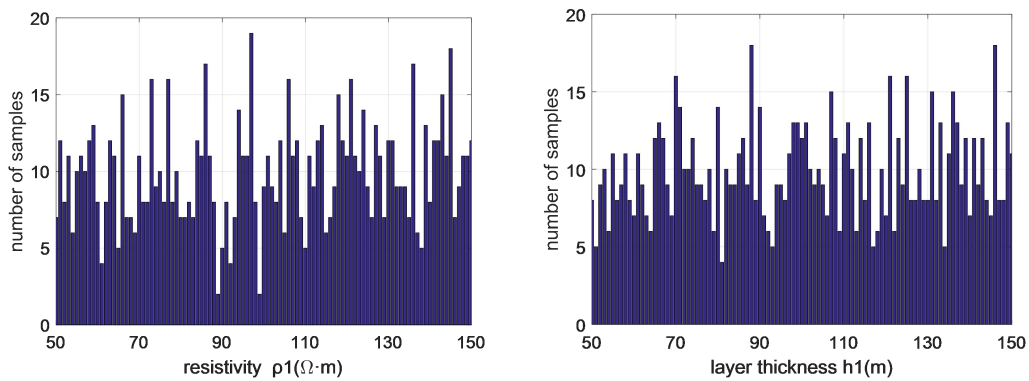
218 4.3 Layered model inversion

219 A 3-layered and 5-layered geoelectric models were investigated, which the PSO parameter values
 220 are the same as those of the Algorithm Testing parts in the paper. In order to simulate actual TEM
 221 applications, the ramp turn-off is taken into account. Considering the probability distribution
 222 characteristic of above algorithms, the average of 20 simulation results is chosen. The BP,
 223 SPSO-BP, COPSO-BP algorithms and non-linear programming genetic algorithm (NPGA) (Li et
 224 al., 2017) were compared.

225 (1) 3-layered H type model

226 The central loop TEM parameters are set as following, transmitting coil radius $a = 100$ m, ramp
 227 emission current is 100 A, turn-off time is 1 μ s. In the geoelectric model, the resistivity $\rho_1 = 100$
 228 $\Omega \cdot m$, $\rho_2 = 10 \Omega \cdot m$, $\rho_3 = 100 \Omega \cdot m$ and thickness $h_1 = 100$ m, $h_2 = 200$ m.

229 The BP training samples which is a series of $H_z(t)$ for different geoelectric parameters were
 230 generated by TEM forward model. The resistivity ranges were $\rho_1 \in (50, 150)$, $\rho_2 \in (5, 15)$,
 231 $\rho_3 \in (50, 150)$, the thickness range were $h_1 \in (50, 150)$, $h_2 \in (100, 300)$, and choosing 1000 random
 232 groups. The resistivity and thickness distributions of ρ_1 and h_1 were shown in Fig.6.



233
 234 **Fig. 6** Distribution of resistivity ρ_1 and thickness h_1 in training samples

235 The inversion results were shown in Table.4. and Fig.7~8. The BP type algorithms were
 236 superior to the NPGA inversion in Table.4. Moreover, the inversion accuracy, convergence rate
 237 and optimization ability of the COPSO-BP algorithm were better than others.

Table.4 Inversion comparison of three-layer H type geoelectric model

H type	resistivity ρ ($\Omega \cdot m$)			thickness $h(m)$		total relative error(%)
	ρ_1	ρ_2	ρ_3	h_1	h_2	
reference value true values	100	10	100	100	200	--
BP relative error(%)	-0.275	-0.625	0.765	-0.968	-0.649	3.284
SPSO-BP relative error(%)	0.062	-0.322	-0.737	-0.579	-0.970	2.672
COPSO-BP	100.031	9.991	99.310	100.234	200.886	--
COPSO-BP relative error(%)	0.031	-0.087	-0.689	0.234	0.443	1.487
NPGA relative error(%)	0.133	-0.034	3.450	-7.305	-0.401	11.323

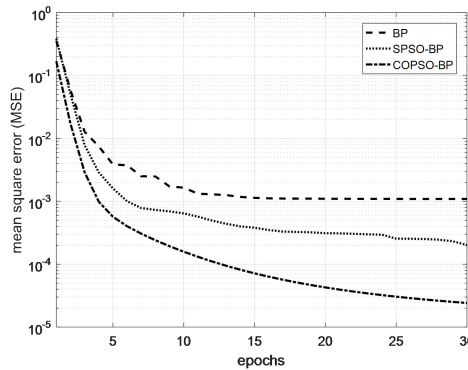
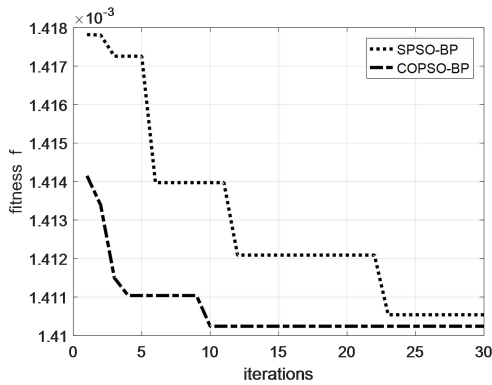


Fig. 7 Fitness curves of SPSO-BP and COPSO-BP **Fig. 8** Mean square error curves comparison

Additional results showed that the solution range of ρ_1 and h_1 in 20 times simulations for above algorithms were $\rho_1 \in (97.980, 103.102)$, $h_1 \in (96.962, 102.480)$ for BP, $\rho_1 \in (98.954, 101.137)$, $h_1 \in (96.955, 101.829)$ for SPSO-BP, $\rho_1 \in (99.382, 100.989)$, $h_1 \in (97.877, 101.044)$ for COPSO-BP respectively. Therefore, the COPSO-BP can acquire higher accuracy and is more stable.

(2) 5-layered KHK type model

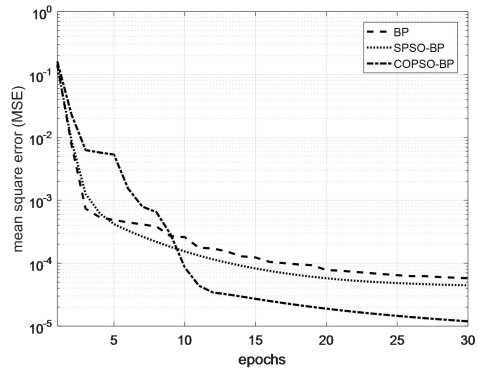
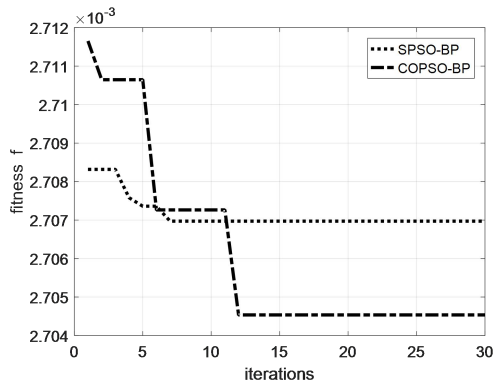
A 5-layered KHK type geoelectric model was adopted and its resistivity were $\rho_1 = 100 \Omega \cdot m$, $\rho_2 = 300 \Omega \cdot m$, $\rho_3 = 50 \Omega \cdot m$, $\rho_4 = 200 \Omega \cdot m$, $\rho_5 = 30 \Omega \cdot m$ and thickness were $h_1 = 100 m$, $h_2 = 200 m$, $h_3 = 300 m$, $h_4 = 500 m$.

The training samples with parameter ranges were $\rho_1 \in (50, 150)$, $\rho_2 \in (150, 450)$, $\rho_3 \in (25, 75)$, $\rho_4 \in (100, 300)$, $\rho_5 \in (15, 45)$ for resistivity, and $h_1 \in (50, 150)$, $h_2 \in (100, 300)$, $h_3 \in (150, 450)$, $h_4 \in (250, 750)$ for thickness. The 1000 groups training samples were generated within above ranges. The inversion results were shown in Table.5 and Fig.9~10. As can be seen that the COPSO-BP algorithm has better global optimization performance.

Table.5 Inversion comparison for five-layer KHK type geoelectric model

KHK type	resistivity $\rho(\Omega \cdot m)$					thickness $h(m)$				Total relative error(%)
	ρ_1	ρ_2	ρ_3	ρ_4	ρ_5	h_1	h_2	h_3	h_4	

reference value	100	300	50	200	30	100	200	300	500	--
BP relative error(%)	-1.006	-0.862	-1.014	-0.030	1.119	-0.362	-0.298	-0.575	-0.376	5.645
SPSO-BP relative error(%)	0.429	1.040	-0.577	-0.071	-0.883	-0.002	0.657	-0.655	-0.316	4.634
COPSO-BP	99.594	299.469	50.082	199.092	29.937	99.501	200.481	301.800	497.670	--
COPSO-BP relative error(%)	-0.405	-0.176	0.164	-0.453	-0.209	-0.498	0.240	0.600	-0.465	3.214
NPGA relative error(%)	-6.211	-0.008	-0.974	3.930	3.083	-0.691	0.505	-2.900	-3.370	19.062



255

256

Fig. 9 Fitness curves of SPSO-BP and COPSO-BP

Fig. 10 Mean square error curves comparison

257

(3) Inversion comparison

258

Three kinds of BP methods as traditional BP, the SPSO-BP and the COPSO-BP algorithms were compared in Table.6. Hence, the training times of COPSO-BP was obviously less than SPSO-BP and was almost equal to BP, it can obtain better precision especially for its global optimization performance.

259

260

261

262

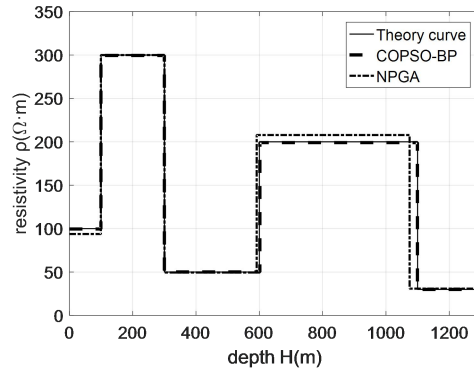
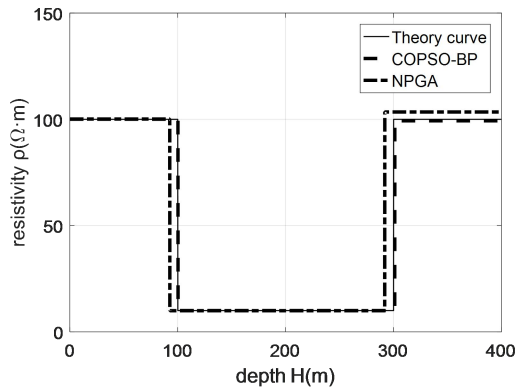
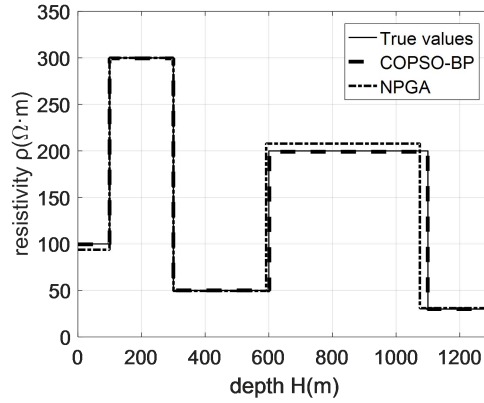
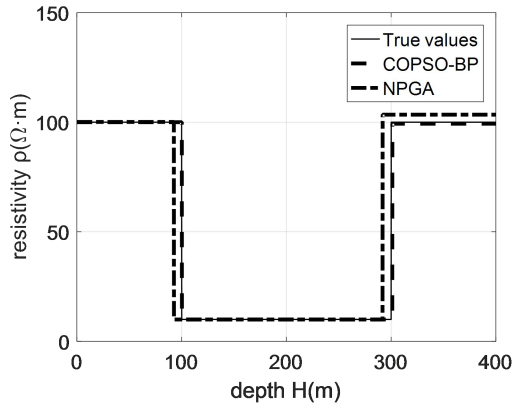
Table.6 Simulation comparison for different algorithms

inversion method	three-layer H type model			five-layer KHK type model		
	training times	minimum training error	test relative error rate(%)	training times	minimum training error	test relative error rate(%)
BP	3	0.2882	3.284	5	0.3013	5.645
SPSO-BP	7	0.2832	2.672	15	0.2992	4.634
COPSO-BP	5	0.2725	1.487	6	0.2900	3.214

263

The inversion of COPSO-BP and NPGA were compared in Fig.11. The fitting ability of COPSO-BP was much better than NPGA.

264



(a) Three-layer H type geoelectric model

(b) Five-layer KHK type geoelectric model

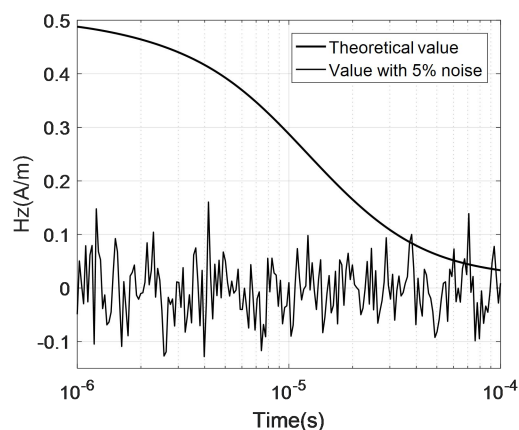
Fig. 11 Inversion comparison for different geoelectric models

(4) Robust performance analysis

In order to verify the algorithm robustness, 5%(26dB) and 10%(20dB) Gaussian random noise was added in TEM data for three-layer geoelectric model. Three kinds of inversions were implemented respectively. The results and comparison were shown in Table.7. The $H_A(t)$ and data with 5% noise were shown in Fig.12.

Table 7 Comparison of inversion results for three-layer H type (with noise) model

model parameters	resistivity $\rho(\Omega \cdot m)$			thickness $h(m)$		Total relative error(%)	
	ρ_1	ρ_2	ρ_3	h_1	h_2		
true value	100	10	100	100	200	--	
without noise	BP	99.724	9.937	100.765	99.031	198.701	3.284
	COPSO-BP	100.031	9.991	99.310	100.234	200.886	1.487
5% noise	BP	101.374	9.966	98.283	101.255	199.282	5.039
	COPSO-BP	100.252	9.977	98.222	101.206	199.228	3.847
10% noise	BP	90.525	9.931	99.481	101.748	203.105	13.976
	COPSO-BP	104.472	9.96050	101.345	100.570	199.437	7.064



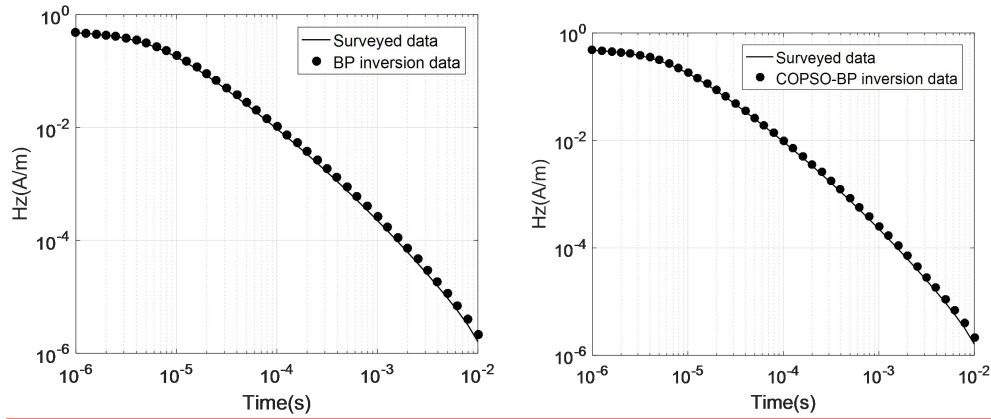
275

276 **Fig.12 Forward data of Hz and data with 5% noise**

277 As can be seen from Table 3, after applying 5% and 10% Gaussian noise the COPSO-BP
 278 inversion has higher robust ability. The accuracy was obviously improved based on the total
 279 relative error data.

280 **4.4 Field example**

281 In order to test the effectiveness of the method, a transient electromagnetic vertical magnetic field
 282 (Hz) with 10 measuring points at the 380m to 1280m of the No. 1 line from a mining area in
 283 Anhui Province was selected. After the data processing, the inversion was performed using the
 284 3-layer neural network model in the previous section, and the results of BP and COPSOBP
 285 inversion were compared. Figure 13 shows the comparison between the surveyed data and the
 286 inversion data at 380m of the No. 2 line in the mining area. Figure 14 displays the pseudo-sections
 287 of the 10 sets of inversion data combined with the geological data interpolation smoothing. It can
 288 be seen from Fig. 14 that the first layer is a low resistivity (100~200 $\Omega \cdot m$), which is inferred to be
 289 the second layer (T2g22) gray dolomite of the Middle Triassic old Malague section, with a
 290 thickness of about 200 m; the second layer is the second highest resistivity (300~400 $\Omega \cdot m$), which
 291 is surmised to be the first layer (T2g21) dolomite of the Middle Triassic old Malaga section, with a
 292 thickness of about 400m; the third layer is high resistivity (600~800 $\Omega \cdot m$), which is speculated to
 293 be the 6th layer (T2g16) limestone dolomite of the Middle Triassic old group. The results are
 294 basically consistent with the geological conditions of the mining area, indicating the feasibility
 295 and effectiveness of the neural network method. And the results of COPSO-BP inversion are better
 296 than those of BP, which the inversion position is more accurate, the shape and spacing are clearer,
 297 and the resistivity of each layer is more consistent with the those of the actual geological model.



298

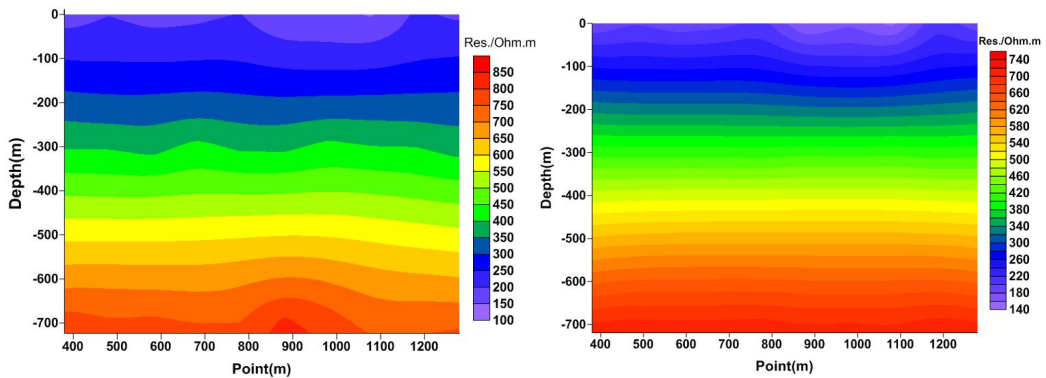
(a) BP

(b) COPSOBP

299

300

Figure 13. 1D inversion forward results. (a) BP; (b) COPSOBP.



301

(a) BP

(b) COPSOBP

302

303

Figure 14. Inversion results of BP (a) and COPSOBP (b).

304

5 Discussion

305

The inversion is performed for 3-layered (H-type) and 5-layered (KHK-type) geoelectric models

306

in this paper. The results show that the BP neural network is better than the NPGA algorithm,

307

because the BP method does not need to use the forward algorithm repeatedly, and its calculation

308

time is short, which is different from the nonlinear heuristic method based on global space search

309

solution.

310

The BP main advantage is that it can interpret the transient electromagnetic sounding results

311

quickly after training the network. Furthermore, BP algorithm could automatically obtain the

312

"reasonable rules" between input and output data by learning, and it can adaptively store the

313

learning content in the network weight, which the BP neural network has the high self-learning

314

and self-adaptation ability. In addition, the superior simulation results of the test function indicate

315

that the BP algorithm can approximate any nonlinear continuous function with arbitrary precision,

316

which means it has strong nonlinear mapping ability; the inversion results of the layered

317

geoelectric model with uncorrelated noise data prove that the BP algorithm has strong robustness.

318 which means it has the ability to apply learning results to new knowledge. However, the BP neural
319 network weight is gradually adjusted by the direction of local improvement, which causes the
320 algorithm to fall into local extremum, and the weight converges to a local minimum that leads to
321 the network training failure; Moreover, BP is very sensitive to the initial network weight, and the
322 initialization network with different weight values tends to converge to different local minimums,
323 so that obtains different results each time; In addition, the BP algorithm is a gradient descent
324 method essentially, which leads to a slow convergence rate.

325 From the results of the layered model and parametric analysis part, it can be seen that single
326 BP algorithm has higher error value than SPSO-BP, because BP method is sensitive to initial
327 weight and easy to fall into local minimum values, thus a heuristic global search particle swarm
328 optimization algorithm with simple structure, rapid convergence and high precision is applied to
329 optimize the weight and threshold of BP neural network, which improves the global optimization
330 performance of the algorithm. Furthermore, the PSO algorithm adjusts the inertia weight
331 adaptively based on the chaotic oscillation curve that is similar to the annealing process in the
332 simulated annealing algorithm (SA), which jumps out the local extremum faster in the early stage
333 and accelerates the convergence and reduces the training times. Therefore, compared with
334 SPSO-BP and BP algorithm, the inversion results of COPSO-BP are closer to the theoretical data
335 with smaller error fluctuations, stronger anti-noise, better generalization performance and higher
336 stability, which it is effective in solving geophysical inverse problems.

337 From the simulation experiment, it is not clear how the weight organization affects the BP
338 neural network weight learning process. It is necessary to conduct a more systematic study on this
339 problem to improve our understanding of how BP neural network handles training data.

340 **65 Conclusion**

341 The nonlinear COPSO-BP method was proposed for TEM inversion. The BP's initial weight and
342 threshold parameters were trained by COPSO algorithm which makes it not easy to fall into local
343 optimum. The chaotic oscillation inertia weight for PSO was proposed so as to improve the PSO's
344 global optimization ability and fast convergence in early stage. The layered geoelectric model
345 inversion showed that the COPSO-BP method has better accuracy, stability and relative less
346 training times.

347

348 **Author Contributions**

349 Huaqing Zhang conceived this manuscript. Huaqing Zhang and Ruiyou Li developed the main
350 algorithmic idea and mathematical part. Ruiheng Li and Nian Yu carried out the simulation and
351 data analysis. Qiong Zhuang completed the writing and interpretation of this manuscript. All
352 authors contributed to the manuscript writing and approved the final manuscript.

353

354 **Competing interests**

355 The authors declare that they have no conflict of interest.

356

357 **Acknowledgments**

358 This work was partly supported by the National Natural Science Foundation of China
359 (No.51377174, No.51577016, No.51877014), the Fundamental Research Funds for the Central
360 Universities(No.2018CDQYDQ0005).

361 **Computer Code Availability**

362 Code name is PSOBP, developer is Huaiqing Zhang and Ruiyou Li, contact address is
363 Chongqing University in China, telephone number is 13752954568 and e-mail is
364 zhanghuaiqing@cqu.edu.cn, year first available, hardware required is a computer, software
365 required is MATLAB R2016a, program language is C++, program size is 10KB, and source code
366 from <https://github.com/liruiyou/PSOBP>.

367 **Reference**

368 Dai, Q., Jiang, F., and Dong, L.: Nonlinear inversion for electrical resistivity tomography based on chaotic DE-BP
369 algorithm, *J. Cent. South. Univ.*, 21, 2018-2025, <https://doi.org/10.1007/s11771-014-2151-9>, 2014.

370 Fernández Martínez, J. L., García Gonzalo, E., Fernández Álvarez, J. P., Kuzma, H. A., and Menéndez Pérez, C. O.:
371 PSO: A powerful algorithm to solve geophysical inverse problems: Application to a 1D-DC resistivity case,
372 *Journal of Applied Geophysics*, 71, 13-25, <https://doi.org/10.1016/j.jappgeo.2010.02.001>, 2010.

373 Godio, A., and Santilano, A.: On the optimization of electromagnetic geophysical data: Application of the PSO
374 algorithm, *Journal of Applied Geophysics*, 148, 163-174, <https://doi.org/10.1016/j.jappgeo.2017.11.016>, 2018.

375 Wang, H., Liu M. L., Xi, Z. Z., Peng, X. L., He, H.: Magnetotelluric inversion based on BP neural network
376 optimized by genetic algorithm, *Chinese Journal of Geophysics*, 61, 1563-1575 [https://doi.org/10.6038/cjg](https://doi.org/10.6038/cjg2018L0064)
377 2018L0064, 2018.

378 Jha, M. K., Kumar, S., and Chowdhury, A.: Vertical electrical sounding survey and resistivity inversion using
379 genetic algorithm optimization technique, *J. Hydrol.*, 359, 71-87, <https://doi.org/10.1016/j.jhydrol.2008.06.018>,
380 2008.

381 Jiang, F., Dai, Q., and Dong, L.: An ICPSO-RBFNN nonlinear inversion for electrical resistivity imaging, *J. Cent.*
382 *South. Univ.*, 23, 2129-2138, <https://doi.org/10.1007/s11771-016-3269-8>, 2016a.

383 Jiang, F., Dai, Q., and Dong, L.: Nonlinear inversion of electrical resistivity imaging using pruning Bayesian
384 neural networks, *Journal of Applied Geophysics*, 13, 267-278, <https://doi.org/10.1007/s11770-016-0561-1>,
385 2016b.

386 Jiang, F., Dong, L., and Dai, Q.: Electrical resistivity imaging inversion: An ISFLA trained kernel principal
387 component wavelet neural network approach, *Neural. Networks.*, 104, 114-123, [https://doi.org/10.1016/j.neunet.](https://doi.org/10.1016/j.neunet.2018.04.012)
388 2018.04.012, 2018.

389 Kaufman, A. A., and Keller, G. V.: Frequency and Transient Sounding, Elsevier Methods in Geochemistry &
390 Geophysics, 1983.

391 Johnson, O. L., Aizebeokhai, A. P.: Application of Artificial Neural Network for the Inversion of Electrical
392 Resistivity Data, Journal of Informatics and Mathematical Sciences, 9, 297-316, 2017.

393 Li, F. P., Yang, H. Y., and Liu, X. H.: Nonlinear programming genetic algorithm in transient electromagnetic
394 inversion, Geophysical and Geochemical Exploration, 41, 347-353, 2017.

395 Maiti, S., Erram, V. C., Gupta, G., and Tiwari, R. K.: ANN based inversion of DC resistivity data for groundwater
396 exploration in hard rock terrain of western Maharashtra (India), J. Hydrol., 464, 294-308,
397 <https://doi.org/10.1016/j.jhydrol.2012.07.020>, 2012.

398 Pekşen, E., Yas, T., and Kıyak, A.: 1-D DC Resistivity Modeling and Interpretation in Anisotropic Media Using
399 Particle Swarm Optimization, Pure. Appl. Geophys., 171, 2371-2389,
400 <https://doi.org/10.1007/s00024-014-0802-2>, 2014.

401 Raj, A. S., Srinivas, Y. , and Oliver, D. H.: A novel and generalized approach in the inversion of geoelectrical
402 resistivity data using Artificial Neural Networks (ANN), J. Earth Syst. Sci., 123, 395-411,
403 <https://doi.org/10.1007/s12040-014-0402-7>, 2014.

404 Rosas-Carbajal, M., Linde, N., Kalscheuer, T., and Vrugt, J. A.: Two-dimensional probabilistic inversion of
405 plane-wave electromagnetic data: methodology, model constraints and joint inversion with electrical resistivity
406 data, Geophys. J. Int., 196, 1508-1524, <https://doi.org/10.1093/gji/ggt482>, 2014.

407 Shi, F., Wang, X. C., and YUN L.: Matlab neural network case study, The Beijing University of Aeronautics &
408 Astronautics Press, Beijing, 2010.

409 Sharma, S. P.: VFSARES—a very fast simulated annealing FORTRAN program for interpretation of 1-D DC
410 resistivity sounding data from various electrode arrays, Comput. Geosci., 42, 177-188,
411 <https://doi.org/10.1016/j.cageo.2011.08.029>, 2012.

412 [Shi, X. M., Xiao, M., Fan, J. K., Yang, G. S., and Zhang, X. H.: The damped PSO algorithm and its application for](#)
413 [magnetotelluric sounding data inversion, Chinese Journal of Geophysics., 52, 1114–1120,](#)
414 <https://doi.org/10.3969/j.issn.0001-5733.2009.04.029>, 2009.

415 Srinivas, Y., Raj, A. S., Oliver, D. H., Muthuraj, D., and Chandrasekar, N.: A robust behavior of Feed Forward
416 Back propagation algorithm of Artificial Neural Networks in the application of vertical electrical sounding data
417 inversion, Geosci. Front., 3, 729-736, <https://doi.org/10.1016/j.gsf.2012.02.003>, 2012.

418 Tran, K. T., and Hiltunen, D. R.: Two-Dimensional Inversion of Full Waveforms Using Simulated Annealing, J.
419 Geotech. Geoenviron. Eng., 138, <https://doi.org/1075-1090>, 2012.

420 Li, Y. Y., Chen, B. C., Zhao, Y. G., Yun, C., Ma, X. B., and Kong, X. R.: Nonlinear inversion for electrical
421 resistivity tomography, Chinese Journal of Geophysics, 52, 758-764,
422 [https://doi.org/10.1016/S1003-6326\(09\)60084-4](https://doi.org/10.1016/S1003-6326(09)60084-4), 2009.

423 Zhang, L. Y., and Liu, H. F.: The application of ABP method in high-density resistivity method inversion, Chinese
424 Journal of Geophysics., 54, 64-71, <https://doi.org/10.1002/cjg2.1587>, 2011.